Surface Microphysical Observations within East Coast Winter Storms on Long Island, New York

BRIAN A. COLLE

School of Marine and Atmospheric Sciences, Stony Brook University, Stony Brook, New York

DAVID STARK

NOAA/National Weather Service, New York, New York

SANDRA E. YUTER

Department of Marine, Earth, and Atmospheric Sciences, North Carolina State University, Raleigh, North Carolina

(Manuscript received 26 January 2014, in final form 24 April 2014)

ABSTRACT

Surface observations of ice habit and degree of riming were measured for 12 cyclone events over 3 winter seasons at Stony Brook, New York, on the northeast coast of the United States. A total of 205.6 cm of snow accumulated during these storms, with an average degree of riming of 1.25 (out of 5) and snow-to-liquid ratio ranging from 3:1 to 17:1. There were consistent spatial patterns of habit and riming intensity relative to the cyclone structure. Cold-type habits (side planes and bullets) commonly occurred within the outer comma head to the north and northeast of the cyclone center. In the middle of the comma head, moderately rimed dendrites, plates, and needles were observed. Close to the cyclone center, heavy riming was observed with needles and graupel. The western quadrant of the comma head had primarily plates and dendrites with little to no riming. Periods of light riming and high snow–liquid ratios (≥13:1) are dominated by cold-type habits, dendrites, and plates and have similar vertical motion and synoptic characteristics inferred from 13-km Rapid Update Cycle analyses. Maximum vertical motion occurred in a region of favored ice growth and less supercooled water (from −15° to −25°C). During heavy riming periods, needles and graupel are dominant and the vertical motion maximum occurs at temperatures from 0° to −5°C. Vertically pointing Micro Rain Radar indicates stronger vertical motions and turbulence for heavy riming as opposed to light rimming periods. Periods with low snow-to-liquid ratio (≤7:1) were observed to occur either as heavy rimed particles or as light riming of compact habits such as sideplanes, bullets, and needles.

1. Introduction

a. Background

Accurate forecasting of snowfall amount is a challenging problem. High-resolution numerical models can realistically predict the precipitation structures within winter extratropical cyclones (Novak et al. 2008; Novak and Colle 2012; Brown et al. 1999), but there are large uncertainties in model microphysics for these storms (Molthan and Colle 2012; Lin and Colle 2011; Garvert et al. 2005). In-cloud temperatures, relative humidity, and vertical air motions determine ice crystal habit or sequence of habits, aggregation, and/or riming. Snow can also be modified as it falls below cloud and by surface conditions once it reaches the ground (Roebber et al. 2003). The snow density is dependent on the ice habits and their sizes (Ryan et al. 1976; Takahashi et al. 1991), sublimation and melting as the crystals fall (Roebber et al. 2003), degree of riming (Power et al. 1964; Locatelli and Hobbs 1974), and compaction at ground level (Roebber et al. 2003). The ice crystal habit is determined by the amount of supersaturation and temperature (Magono and Lee 1966; Hobbs 1975; Stoelinga et al. 2007; Bailey and Hallett 2009).

Ice habits are not considered in most bulk microphysical schemes, and the degree of riming has only been recently introduced in model microphysical

Corresponding author address: Dr. Brian A. Colle, School of Marine and Atmospheric Sciences, Stony Brook University, Stony Brook, NY 11794-5000.
E-mail: brian.colle@stonybrook.edu

DOI: 10.1175/MWR-D-14-00035.1

parameterizations (Lin and Colle 2011). Operationally, empirical statistical approaches are commonly used to predict snow density, which can vary from as high as $\sim$290 kg m^{-3} (2.9:1 snow-to-liquid ratio) to as low as $\sim$10 kg m^{-3} (100:1 snow-to-liquid ratio) (Power et al. 1964; Super and Holroyd 1997; Judson and Doesken 2000; Roebber et al. 2003; Alcott and Steenburgh 2010). For example, Roebber et al. (2003) examined surface conditions and profiles of temperature and relative humidity to develop an empirical method for predicting snow density. They account for the likelihood of heavy riming indirectly, in terms of the relative humidity at low- and midlevels since their dataset did not include vertical motions. Alcott and Steenburgh (2010) used a stepwise multiple linear regression approach using analysis temperature, wind, and midlevel relative humidity data at Alta, Utah, which could explain 68% snow-to-liquid ratio variance of all cases.

There have been several studies of cloud microphysics within winter storms using aircraft and other data sources. Many of these studies have occurred within mixed phase clouds and either over or adjacent to steep terrain, including the Cascade Project (Hobbs 1975), the Cyclonic Extratropical Storms (CYCLES) project (Houze et al. 1979), Colorado Orographic Seeding Experiment (COSE; Rauber et al. 1986; Rauber 1987), the Sierra Cooperative Pilot Project (SCPP; Reynolds and Dennis 1986; Demoz et al. 1993), the Mesoscale Alpine Programme (MAP; Binder and Schar 1996), and the Improvement of Microphysical Parameterization through Observational Verification Experiment (IMPROVE; Stoelinga et al. 2003). Those studies of precipitation bands within extratropical cyclones have highlighted the ''seeding'' of ice aloft within generating cells for warm frontal bands and the generation of riming and graupel within cold frontal bands (Matejka et al. 1980; Hobbs et al. 1980; Rutledge and Hobbs 1983; Crosier et al. 2014). The studies of orographic snow within these cyclones have found that supercooled water occurs most frequently at lower altitudes above ground level (Rauber et al. 1986; Rauber and Grant 1986; Borys et al. 2003; Garvert et al. 2007).

Along the East Coast of the United States, the terrain is relatively flat compared to the mountainous west coast. Within East Coast storms, the ice habit, riming, and size of precipitation particles within a frontal rainband have been documented using aircraft data (Sienkiewicz et al. 1989). Surface observations made in winter storms in eastern Canada during the Canadian Atlantic Storms Program II (CASP II; Stewart et al. 1995) and the Canadian *CloudSat/Cloud–Aerosol Lidar and Infrared Pathfinder Satellite Observations* (*CALIPSO*) Validation Project (C3VP; Petersen et al. 2007; Molthan et al. 2010; Molthan and Colle 2012) indicated a wide variety of habits and degrees of riming within surface snowfall.

Stark et al. (2013) presented the observed microphysical evolution of two coastal extratropical cyclones (19–20 December 2009 and 12 January 2011) and the associated passage of a heavy snowband in the cyclone comma head. The observations were made approximately 93 km east of New York City (NYC) on the north shore of Long Island (LI) at Stony Brook, New York (SBNY on Fig. 1). They highlighted rapid changes in the ice habit at the surface corresponding to changes in the altitude of maximum vertical motion aloft and associated changes in temperature and habits favored for depositional growth. When the maximum vertical motion was in the $-5°$ to $-10°$C layer, needles were often observed during the preband period. Stronger vertical motion on the warm (east) side of the snowband at temperatures from $-12°$ to $-15°$C resulted in moderately rimed dendritic crystals. Postband, riming rapidly decreased and the habits were more platelike as the magnitude of maximum ascent between $-12°$ and $-15°$C weakened.

b. Motivation

To improve precipitation forecasts and model bulk microphysical parameterizations (BMPs) regarding the ice habit and degree of riming, more in situ observations of ice microphysics within winter storms are needed. Few studies have investigated the ice habit, riming, snow density, particle fall speed, and size distributions at the surface within U.S. East Coast winter storms. This study extends the results of Stark et al. (2013) by presenting a more comprehensive analysis that summarizes all the microphysical observations collected in 12 storms during the 2009–10, 2010–11, and 2011–12 winter seasons (Table 1).

This study combines observations of surface snow and a vertically pointing radar with model output over the SBNY observation site to describe where and when different types of snow can occur within a winter cyclone structure. It is hypothesized that the surface ice habit, snow-to-liquid water ratios, and riming at SBNY can be related to changes in vertical motion and temperature aloft as an extratropical cyclone develops and approaches. With the 12 events in this study, there is not enough data to obtain statistically significant relationships among all of these parameters. The 12 events analyzed show some consistent patterns among storms. This analysis represents an initial step in moving beyond case studies to describe generalities among the common structures modulating snowfall within New York City metro area winter storms.

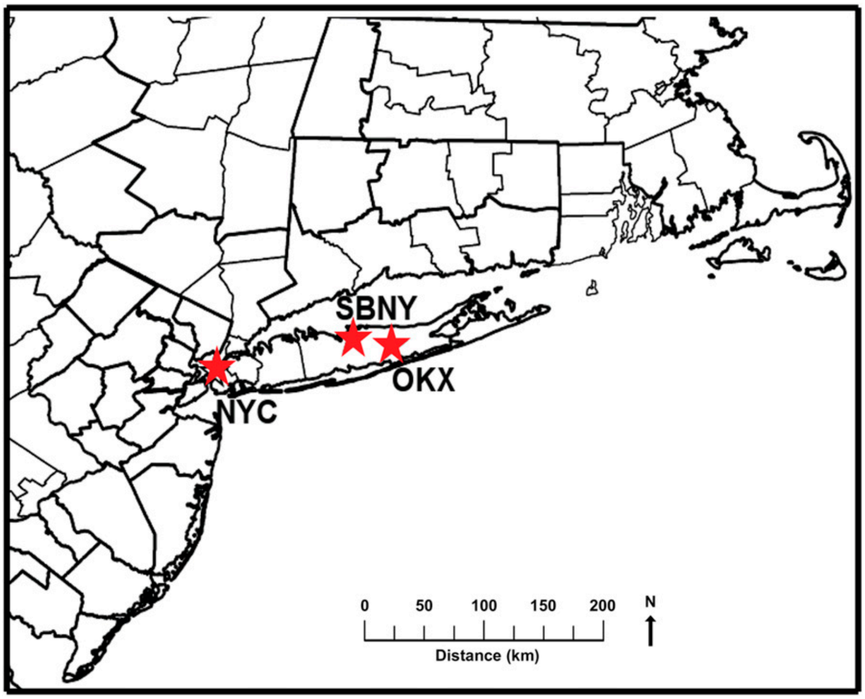

FIG. 1. Location map where the in situ observations were collected (SBNY) and where the closest National Weather Service radar is located (OKX). NYC is highlighted for reference.

This paper will be organized as follows: section 2 will discuss the data and methods used in this study. Section 3 will discuss the spatial patterns of the observed ice habits and degree of riming within the comma head of an extratropical cyclone. Section 4 will address the vertical profile characteristics associated with different degrees of riming and habit types, and section 5 will address the snow-to-liquid water variations. The conclusions are presented in section 6.

2. Data and methods

Microphysical observations for this study were obtained during the 2009–10, 2010–11, and 2011–12 winter seasons (Table 1) at SBNY (Fig. 1). There were a total of 12 cyclones events in which the ice habit degree of riming, and snow densities were observed (Table 1). The methodology for observing snow habit is similar to that of Stoelinga et al. (2007) in the Cascade Mountains and Stark et al. (2013). A stereomicroscope and camera in a cold shed were used to observe the snow habit and riming intensity (Fig. 2). Several samples were obtained and examined on a thick glass plate in each 15–30-min time period. For each measurement, the glass plate was held horizontally outside the shed to collect at least 20–30 crystals. The plate was placed under the microscope and the habits types were determined visually and communicated verbally to a note taker or checked off on paper next to the scope in order to obtain a percentage of each habit type observed. The observed crystals were classified by habit following the 81 types in Magono and Lee (1966). A spreadsheet was constructed for each case in which a percentage was assigned to each of the habit types. Since ice crystals were often fragmented on the plate, either from impact or during their fallout, the fragment was still categorized as one of the pristine habits (e.g., branch of a dendrite = pristine dendrite). Unfortunately, many aggregates broke up on impact with the glass plate, so the degree of aggregation could not be determined. For those aggregates that maintained some structure, we estimated the total number of crystals by noting the size of the aggregate divided by the average size of the crystal. We multiplied an additional factor if the aggregate also had some depth. Most of the time the aggregates were made up of the same habit type. For many storms over 40 habit types were observed, but in order to synthesize the results these habit types were grouped into one of nine categories: needlelike, columns, bullets, dendritic, platelike, side planes, graupel, ice miscellaneous, and sleet.

The average degree of riming was determined following Mosimann et al. (1994, see their Table 1), although instead of using integers from 0 to 5, additional

TABLE 1. The 12 cases where SBNY was located within the comma head of an extratropical cyclone. The cyclone type, number of hours, snow amount (cm), the range and mean degree of riming, and the mean and average snow-to-liquid ratio are also given.

Case	Event type	No. of hours	Snow amount (cm)	Degree of riming	Snow-to-liquid ratio
19–20 Dec 2009	Mature cyclone with heavy snowband	21	48	Mean: 1.17 Range: 0–3.5	Mean: 9:1 Range: 7:1–13:1
3–4 Jan 2010	Mature cyclone; warm advection from north in midlevels	9	7	Mean: 0 Range: 0	Mean: 12:1 Range: 10:1–14:1
10–11 Feb 2010	Developing cyclone stage for first 3 h, then mature cyclone	23	34	Mean: 1.89 Range: 0–4.5	Mean: 7:1 Range: 4:1–10:1
16 Feb 2010	Developing cyclone for first 7 h; mature cyclone for remainder of event	14	10	Mean: 1.9 Range: 0–4.5	Mean: 8:1 Range: 5:1–12:1
26–27 Feb 2010	Mature cyclone	15	28	Mean: 1.5 Range: 0–4	Mean: 12:1 Range: 8:1–17:1
3 Mar 2010	Mature cyclone	5	2	Mean: 0 Range: 0	Mean: 5:1 Range: 5:1
5 Mar 2010	Mature cyclone	3	0.6	Mean: 0 Range: 0	Mean: 7:1 Range: 7:1
12 Jan 2011	Mature cyclone with heavy snowband	12	41	Mean: 2.3 Range: 0–5	Mean: 8:1 Range: 4:1–12:1
21 Jan 2011	Developing cyclone	8	11	Mean: 2.0 Range: 0–5	Mean: 8:1 Range: 7:1–9:1
21 Feb 2011	Developing cyclone	6	12	Mean: 0.2 Range: 0–2	Mean: 13:1 Range: 10:1–16:1
21 Jan 2012	Developing cyclone	10	10	Mean: 2.4 Range: 0–5	Mean: 9:1 Range: 2:1–15:1
11 Feb 2012	Developing cyclone	5	2	Mean: 1.1 Range: 0–3	Mean: 8:1 Range: 7:1–9:1

0.5 values were added in order to get some more detail in the riming evolution. This follows Reinking (1975), who had two separate moderate riming categories rather than just the one in Mosimann et al. (1994). For each measurement time, a riming number was recorded for each habit observed in order to obtain the average riming number and the range of values at each observation time. A time period with an average degree of riming less than or equal to Mosimann et al. scale of 1.5, between 1.5 and 3.5, and greater than 3.5–5 was classified as light, moderate, and heavy riming, respectively. We also designate a no-riming category following Mosimann et al. (1994) and Reinking (1975; 1979). The snow depth and snow density were measured several times during the storm. Snow density was obtained by melting snow that had fallen into a circular pan and measuring the change in snow-to-water volume. For the 12 events in this study, a total of 205.6 cm of snow was measured with an average degree of riming of 1.25 and snow-to-liquid ratio ranging from as low as 3:1 to as high as 17:1.

A vertically pointing METEK Ku-band Micro Rain Radar (MRR; 1.25 cm; Peters et al. 2002) was used at SBNY to observe the vertical profiles of reflectivity, Doppler velocity, and Doppler spectral width at 250-m gate spacing to 7.5 km MSL every minute. The MRR has been used to study snowstorms in several locations (Cha et al. 2009; Keighton et al. 2009; Prat and Barros 2010; Kneifel et al. 2011a,b; Xie et al. 2012; Maahn and Kollias 2012). The MRR data were postprocessed using the method of Maahn and Kollias (2012) to improve data quality and sensitivity. Attenuation effects are generally negligible for snow at the K band (Matrosov 2007) except when the antennas are covered by wet snow (Maahn and Kollias 2012; Stark et al. 2013). Doppler velocity from the MRR represents the sum of particle fall speed and vertical air motion. Both turbulence and differential fall speeds yield can wider Doppler spectral widths in vertically pointing radar data. In snow, turbulence associated with updrafts is usually the larger contributor above the boundary layer (Rinehart 2004). For each of the riming categories, the joint frequency distributions of each of the three radar variables with altitude are examined using contoured frequency by altitude (CFAD) diagrams (Yuter and Houze 1995). Since there was little difference in the CFAD distributions between developing and mature cyclone periods, the cases were combined in order to increase sample size.

Gridded hourly analyses from the 13-km Rapid Update Cycle (RUC; Benjamin et al. 2004) provided information on the synoptic and mesoscale wind,

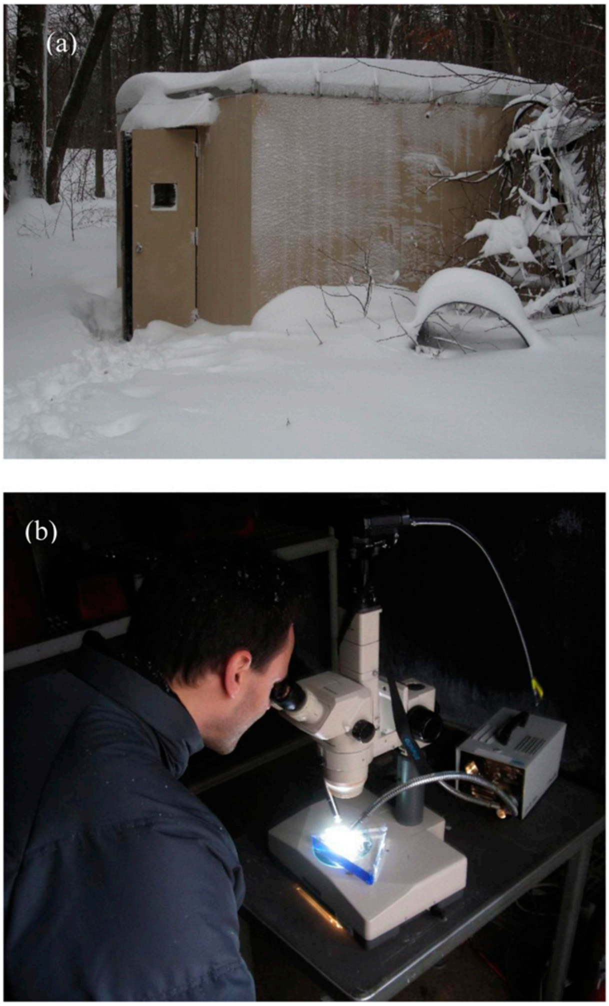

FIG. 2. Photo of the (a) outdoor shed and (b) stereomicroscope, camera, and cold glass plate used during the experiment.

temperature, pressure, and moisture patterns across the region. Hourly analyses from the RUC were also used to construct composites of temperature, vertical motion, moisture, and spatial composites of sea level pressure and 500-hPa height as discussed in section 4. The RUC cannot resolve any convective motions in the cloud, rather it is used to simply represent regions of larger-scale ascent. The 3-hourly surface analyses from the National Weather Service's (NWS's) Weather Prediction Center (WPC) were used to identify the surface synoptic feature related to each observed event.

3. Ice habits and riming within cyclone comma head

The ice habit and riming evolution for the 12 cyclone events are summarized on a schematic of a comma head cloud of an extratropical cyclone (Fig. 3). The location of SBNY relative to the surface cyclone center was determined manually using the NWS's WPC surface analyses, and each time period was then classified as either in the developing cyclone stage or mature stage following the Norwegian and Shapiro and Keyser cyclone models (Bjerknes and Solberg 1922; Shapiro and Keyser 1990). Each event was separated into 2–3-h time periods. The habit icons at a location within the comma head in Fig. 3 show the four most common habits observed in order from more to less frequency at that location. If the average percentage was less than 10%, the habit was not included in this schematic. The average degree of riming for these periods was also included.

Among the 12 events, there were several broad patterns in the habits and degree of riming relative to the cyclone structure. When SBNY was located north of the warm front, mostly moderately rimed needles were observed. Heavily rimed needles and graupel were observed close to the low center. When SBNY was located west-southwest (~100–300 km) of the low center, dendrites and plates were observed with light-to-moderate riming. Overall, there was more variability in dominant habit within the mature cyclone than the developing cyclone. At any given time, multiple habits co-occurred at the surface reflecting both complex microphysical pathways and differential fall speeds of individual hydrometeors.

Within the developing cyclone, the 10 and 16 February 2010 events (Fig. 3a) illustrate that the northern periphery of the comma head was characterized by lightly rimed side planes and bullets (Fig. 4a). Mature cyclone events on 3 March, 10 February, and 3 January 2010 also had primarily side planes (>50%) when SBNY was located along the north outer edge of the comma cloud (Fig. 3b). As the cyclone approached and SBNY entered the middle of the comma head, crystals became moderately rimed with dendrites, plates, and needles (21 January 2011 and 21 January 2012 in Fig. 3a and 26 February and 10–11 February 2010 in Fig. 3b).

When SBNY was relatively close to the low center and just north of the warm front, heavily rimed plates, graupel, and some sleet was observed (Figs. 4d,e). For example, during the 16 February 2010 event the plates and dendrites became progressively more rimed as the surface cyclone approached from the south (Figs. 3a and 4b,c), and there was heavy riming and some graupel observed near the low center. Within the mature cyclones during the 15–16 February 2010 and 12 January 2011 events, moderately rimed plates and dendrites transitioned to heavily rimed needles and graupel (Figs. 3b and 4f) as the midlevel dry intrusion (not shown) approached the surface low center over SBNY.

For the 12 January 2011 event, as the cyclone and associated midlevel dry intrusion shifted east, a heavy snowband developed and there was a transition from

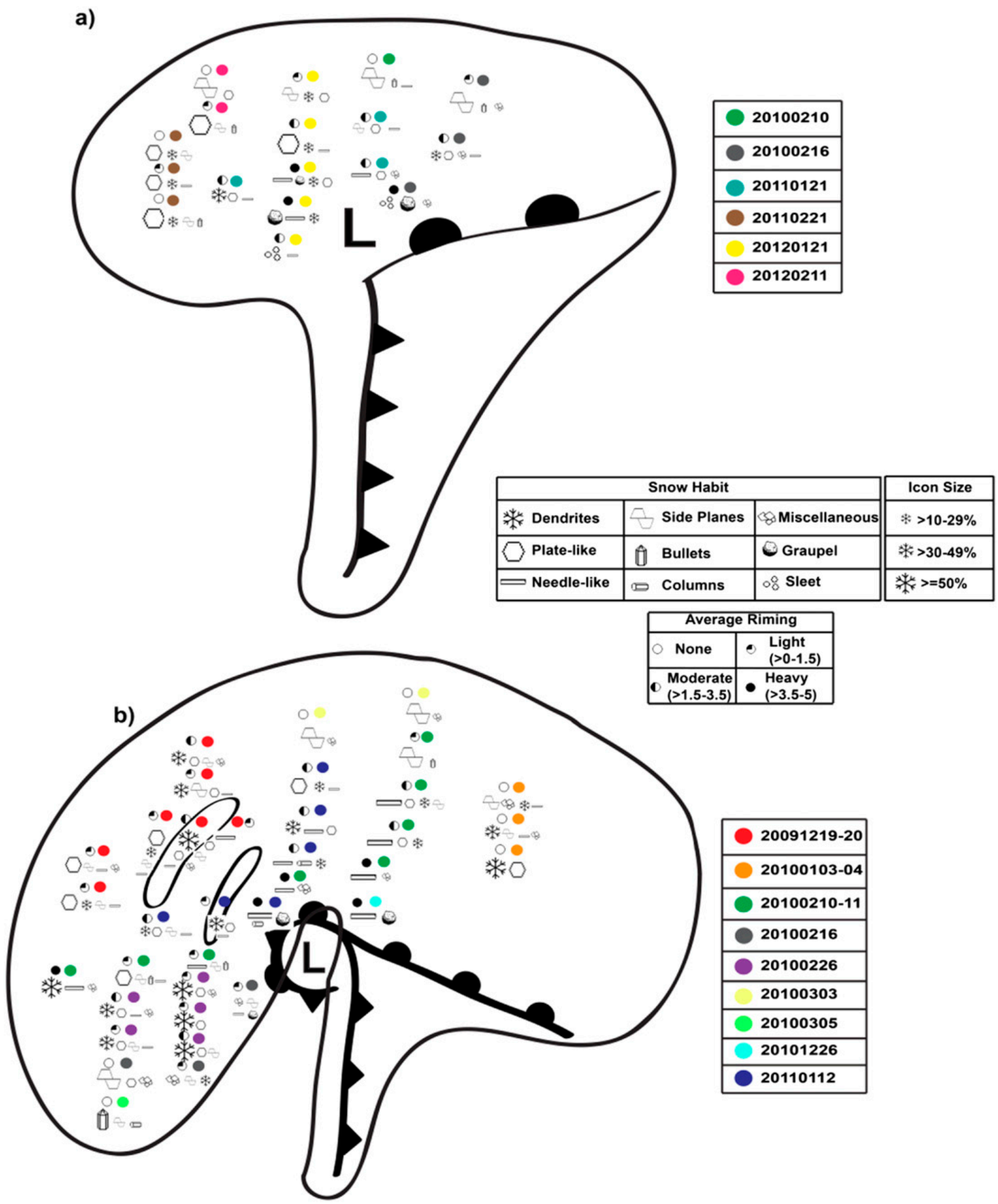

FIG. 3. Observed events classified within the (a) developing cyclone stage and (b) mature cyclone stage following the models given in Bjerknes and Solberg (1922) and Shapiro and Keyser (1990). The habit icons represent the highest four average percentages in order of frequency (from right to left) in each 2–3-h period. The habit percentage is proportional to the size of the symbol as given by the legend. The riming intensity ranges from an open white circle (no riming) to a filled black circle (heavy riming).

heavily rimed needles to lightly rimed dendrites and plates across this band. Another heavy snowband developed during the 19–20 December 2009 event and had a similar evolution from moderate riming and dendrites within the band to lightly rimed plates and dendrites to the west of the band. These heavy snowband characteristics are discussed in Stark et al. (2013).

In the developing cyclone during the 21 February and 21 January 2011 events (Fig. 3a), the western quadrant of the comma head had primarily plates and some dendrites with little to no riming. In the mature cyclones, the region southwest of the low pressure center also had high frequencies of dendrites and plates during the 26 February 2010 storm. During the 16 February 2010

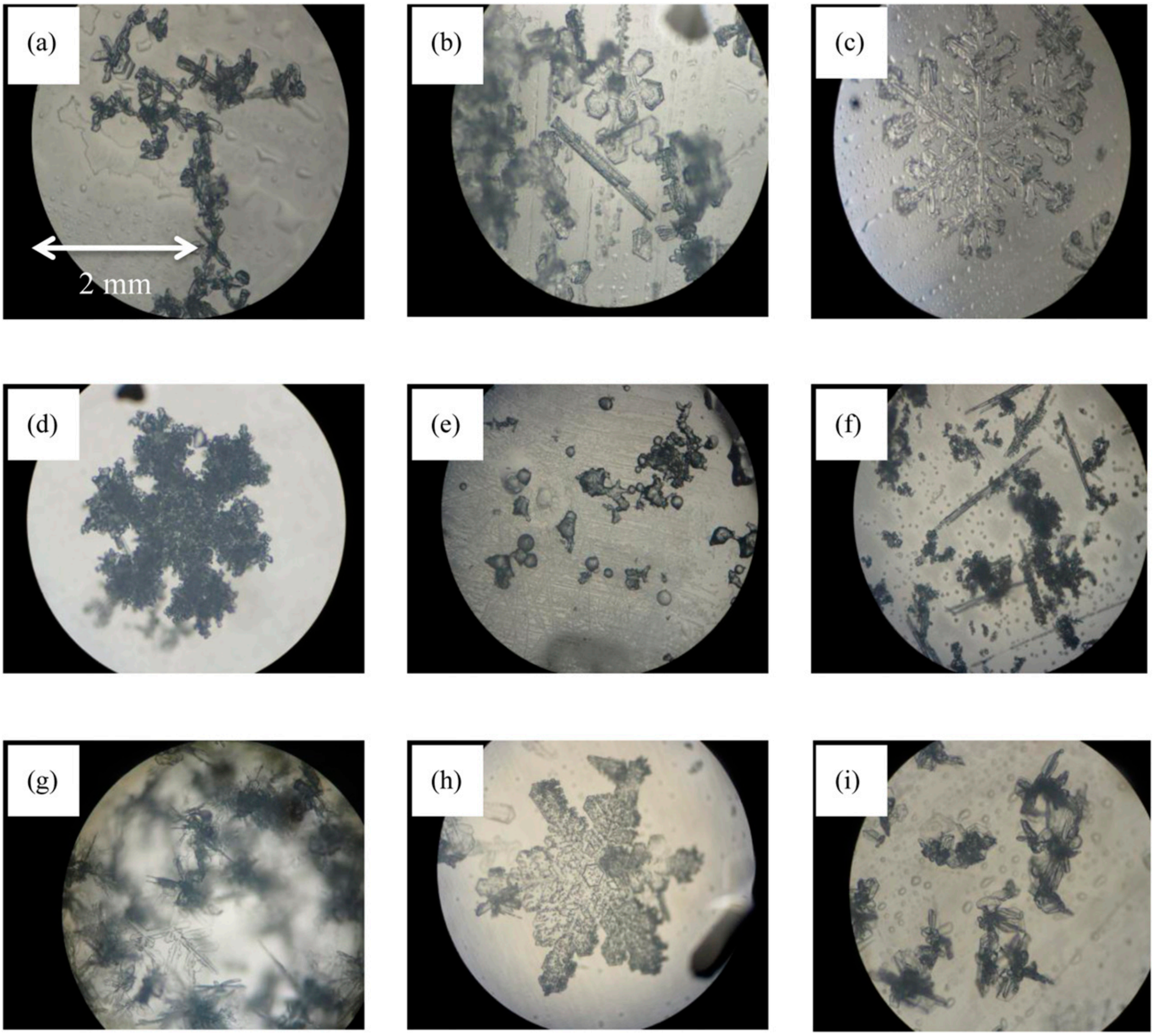

FIG. 4. Observed snow habit from pictures taken under stereomicroscope during the 15–16 Feb event. (a)–(e) Developing cyclone stage and (f)–(i) mature cyclone stage. Some of the crystals are not lying flat and the time represents when crystals were observed at (a) 0145, (b) 0500, (c) 0600, (d) 0630, (e) 0800, (f) 1730, (g) 1830, (h) 1915, and (i) 2200 UTC 16 Feb 2010.

event, as SBNY passes from near the cyclone center (Fig. 3a) to the southwest part of the comma head for the mature cyclone (Fig. 3b), there is a transition from heavily rimed needles and graupel (Fig. 4f) to light-to-moderately rimed dendrites (Figs. 4g,h), and eventually some side planes (Fig. 4i).

Figure 5 shows the observed ice habit percentages for the 12 winter storm events, which is calculated as a percentage of time these habits were observed during these storms. Plates (~23%), dendrites (~20%), side planes (~19%), and needles (12%) were the most frequently observed habits in our sample.

4. Joint ice habit, riming, and profile variations

This section investigates the vertical profiles of temperature and vertical motion associated with different categories of riming. Relative humidity profiles were also compared among habits and riming intensities, but these results are not shown since there was relatively large variability and no clear patterns explaining any riming and habit differences among events. Previous laboratory and field work has determined relationships between ice crystal habit and air temperature (Magono and Lee 1966; Hobbs 1975; Stoelinga et al. 2007; Bailey and Hallett 2009). Supersaturation is also important

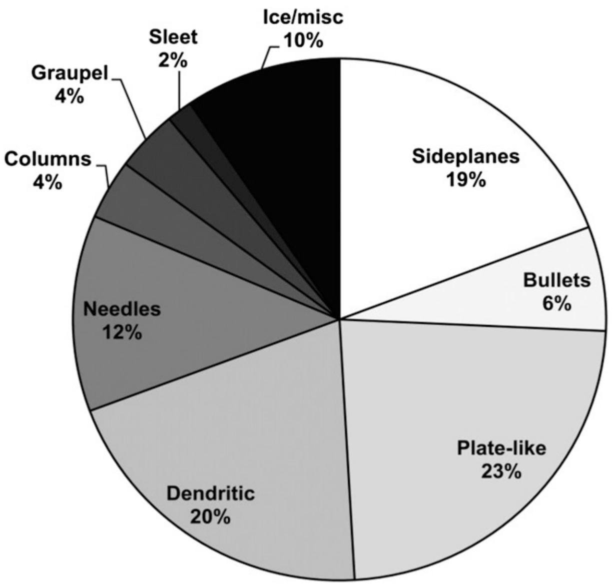

FIG. 5. Observed ice habit percentages from the 2009–10, 2010–11, and 2011–12 winter seasons.

TABLE 2. Time periods for the light, moderate, and heavy riming subsets in the developing and mature cyclones.

Case	Time period (UTC)
Developing cyclones	
Light riming	
10 Feb 2010	0600–0800
16 Feb 2010	0200–0400
21 Feb 2011	0900–1500
21 Jan 2012	0900–1000
11 Feb 2012	0900–1700
Moderate riming	
16 Feb 2010	0500–0600
21 Jan 2011	0700–1300
21 Jan 2012	1100–1200, 1700–1900
Heavy riming	
16 Feb 2010	0700–0900
21 Jan 2012	1300–1600
Mature cyclones	
Light riming	
19–20 Dec 2009	2100–2300, 0000–0200, 0600–1400
3–4 Jan 2010	1800–0300
10–11 Feb 2010	0900–1000, 2100–2300, 0000–0300
16 Feb 2010	1700–2300
26 Feb 2010	1200–2000
3 Mar 2010	0900–1500
5 Mar 2010	1200–1500
12 Jan 2011	1000–1100
Moderate riming	
20 Dec 2009	0300–0500
26–27 Feb 2010	0900–1000, 2100–0000
12 Jan 2011	0200–0500
12 Jan 2011	1200–1500
Heavy riming	
10–11 Feb 2010	1500–2000; 0300–0500
12 Jan 2011	0800–0900

to ice crystal habit (Bailey and Hallett 2009), but we ignore it here in the interest of simplicity and focus on the well-recognized association of temperatures lower than −20°C with side planes and bullets, of temperatures between −20° and −12°C with dendrites and plates, and of temperatures between −10° and −5°C with needles. Columns can grow at multiple temperature levels. By definition, the original habit of the crystal that formed graupel is indistinguishable.

The time periods presented in the cyclone analysis above (Table 1 and Fig. 3) were subset into three degree of riming categories (Table 2). The ice habit percentages within the riming subsets are shown in Fig. 6 for the developing and mature cyclone events. Sleet sometimes coexisted with moderate and heavily rimed crystals and its relative frequency is included in Fig. 6. Figure 6 shows that needles more frequently co-occur with moderate and heavily rimed particles than lightly rimed particles. This is consistent with supercooled water being present at lower altitudes (Rauber et al. 1986; Rauber and Grant 1986; Borys et al. 2003; Garvert et al. 2007). Additionally, the higher formation temperatures (from −10° to −5°C) and lower altitudes associated with needles result in less vertical distance to encounter supercooled water than other particles formed at higher altitudes. Power et al. (1964) suggested that the smaller surface area of the needles as compared to plates and dendrites also limits their ability to rime. Crystals formed at lower temperatures such as side planes and bullets generally decrease in occurrence as the degree of riming increases. It is possible that some graupel originated as side planes or bullets. Since our method only addresses relative frequency of different habits rather than total count of each habit, we cannot determine with this dataset if the total hydrometeor number concentration changes among the riming categories.

Analyses from the RUC were used to construct spatial composites of sea level pressure and 500-hPa height for the times each riming type (light, moderate, and heavy) was observed. The composites were separated into developing and mature cyclones, which can provide some large-scale flow context to the temperature and vertical motion profiles composited for these same events.

a. Light riming

Light riming periods are dominated by a combination of cold-type habits (side planes and bullets), dendrites, and plates in both the developing and mature cyclones

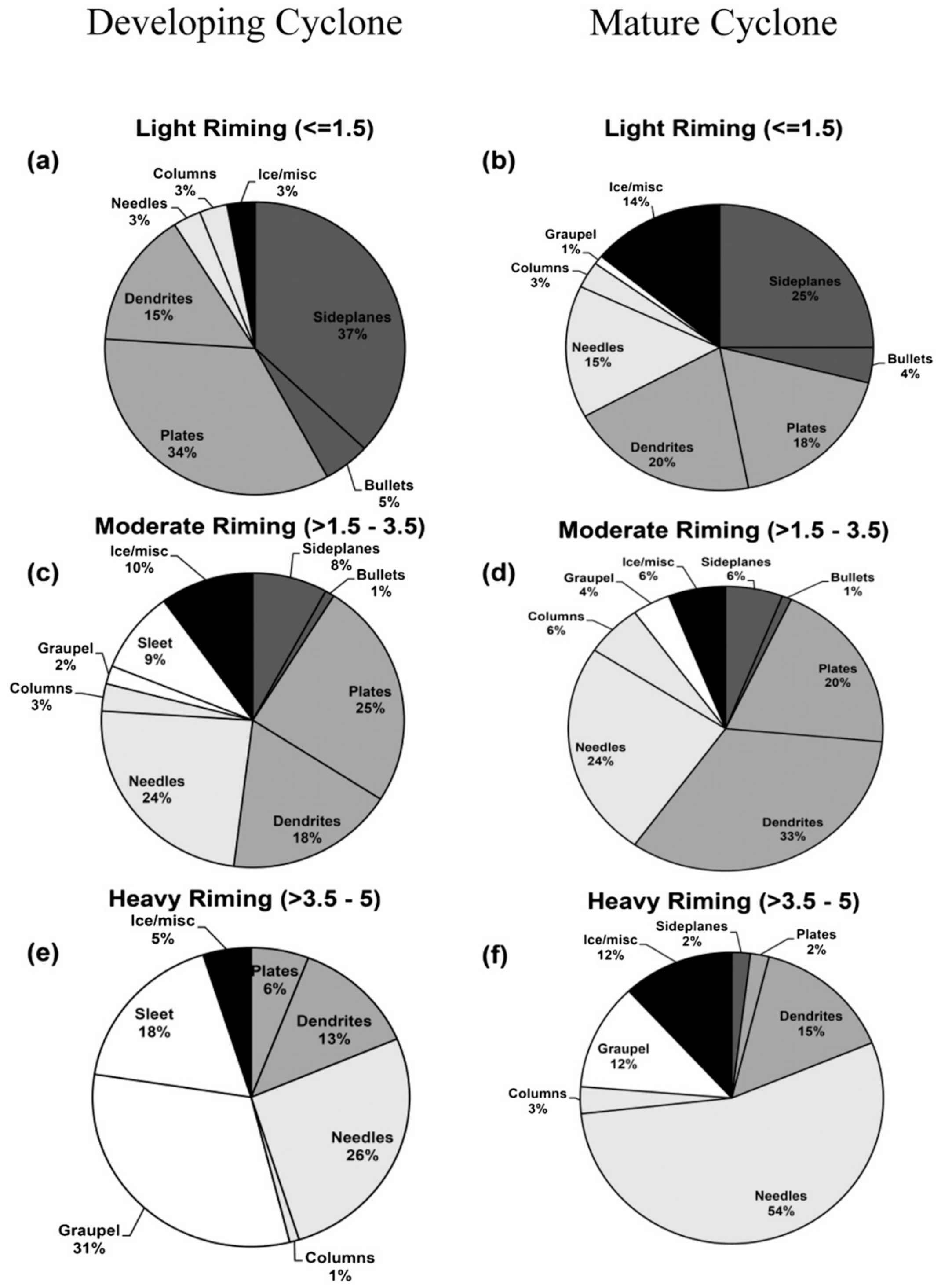

FIG. 6. Observed ice habit percentages during the light riming (≤1.5) time periods for (a) developing and (b) mature cyclone periods. (c),(d) As in (a),(b), but for moderate riming (>1.5–3.5) periods, and (e),(f) for heavy riming (>3.5–5) periods. Cold-type crystals (side planes and bullets) are shaded together, plates and dendrites are shaded together because of their similar growth temperatures, needles and columns are shaded together because of their similar shape, graupel and sleet are shaded the same color because of their similar shape, and ice/miscellaneous are shaded black.

(Figs. 6a,b). Only a small amount (<10%) of relatively warm-type crystal types (growth between −5° and 10°C) are observed in the developing cyclones, while there are more needles and fewer plates in the mature cyclone than in the developing cyclone.

Figure 7 shows a composite analysis of 500-hPa heights and sea level pressure for light riming periods during developing (5 events; Table 2) and mature cyclones (12 events; Table 2). For the developing cyclones (Fig. 7a), there is a 500-hPa shortwave trough centered over the Great Lakes and western Appalachians, while an elongated surface low pressure (1008 hPa) is situated from Pennsylvania to just offshore of the mid-Atlantic states. For the mature cyclones (Fig. 7b), there is a closed 500-hPa low over LI with a deeper (996 hPa) surface low approximately 400 km southeast of SBNY.

Since the location of SBNY is relatively far from the surface cyclone during the light riming composite, the largest ascent is likely at mid- and upper levels given the well-documented warm conveyor belt within that outer part of the comma head (Harrold 1973; Carlson 1980; Browning 1974). A composite vertical profile from 13-km RUC analysis for all light riming periods in developing cyclones shows an average vertical motion maximum (~10 cm s^{-1}) located from 550 to 400 hPa (Fig. 8b), which is associated with temperatures from −15° to −25°C (Fig. 8a). Thus, maximum crystal growth was favored at cold temperatures where there is typically little supercooled water. A deeper layer of vertical motion (~8 cm s^{-1}) is present in the mature cyclones between 450 and 650 hPa (Fig. 8d), where the temperatures in this layer are also between −15° and −25°C (Fig. 8c). Relatively weak vertical motion of ~3–8 cm s^{-1} is also located between −5° and −15°C from 650 and 800 hPa in mature cyclones (Figs. 8c,d).

b. *Moderate riming*

For the moderate riming periods, dendrites and plates are common, occurring just under half the time in the developing cyclones (Fig. 6c) and slightly over half the time in the mature cyclones (Fig. 6d). Needles occur 24% of the time in developing cyclones, and occur ~20% more frequently in moderate and heavy riming than in light riming. In mature cyclones, the amount of needles is also ~24% (Fig. 6d). Meanwhile, cold-type crystals represent less than 10% of the observed habits side planes and bullets for developing and mature storms with moderate riming (Figs. 6c,d).

During moderate riming periods in developing cyclones (four cases; Table 2), the 500-hPa trough is slightly more amplified over the eastern United States than the lightly rimed periods (Fig. 7c), albeit the sample size is relatively small. Meanwhile, the surface low is centered more along the mid-Atlantic coast for the moderate riming than the light riming composite. In mature cyclone periods (five cases; Table 2), the 500-hPa closed low is located over central Pennsylvania and New York rather than over New England for the lightly rimed cases (Fig. 7d). Thus, the surface cyclones are located closer to (~200 km south) SBNY for the moderate rimed events.

With the cyclones closer to SBNY for the moderate riming periods, the strongest upward motion is now located lower in the troposphere. In the developing cyclone, the vertical motion maximum (~8 cm s^{-1}) is between 700 and 900 hPa (Fig. 8b), where it is between −3° and −8°C (Fig. 8a). The average temperature profile above 700 hPa is similar to that in the light riming subset, but the moderate riming periods are ~2°C warmer between 700 and 900 hPa. The vertical motion (~4 cm s^{-1}) is also weaker above 600 hPa for the moderate riming cases. For the mature cyclones, the average vertical motion maximum (~11 cm s^{-1}) (Fig. 8d) is between 500 and 700 hPa, which is from −10° to −20°C (Fig. 8c). The relatively warmer temperatures between 700 and 900 hPa may have allowed for more frequent needles (~24%) in both types of cyclones.

c. *Heavy riming*

Needles and graupel are dominant during heavy riming periods in the developing cyclones (~57%) and mature cyclones (~66%) (Figs. 6e,f). Less than 5% of the crystals are cold type in the developing and mature cyclones, and less than 20% of the habits are dendrites and platelike. About 18% of the habits during developing cyclones are from sleet, while irregular ice is around ~12% for observations within mature storms.

In a limited sample of heavy riming periods (two for developing cyclones, three for mature cyclones; Table 2), the location of the developing surface cyclone and upper-level trough over the eastern United States is similar to the moderate and lightly riming periods (Figs. 7e,f). Therefore, the pressure field does little to distinguish the light and heavy riming cases for developing cyclones. Temperatures between 700 and 900 hPa are ~1°C warmer than the moderate riming profile (Fig. 8a) with a vertical motion maximum of ~13 cm s^{-1} at 800 hPa (Fig. 8b) for the developing cyclones. Around 800 hPa, the variation of the warmer temperatures and enhanced vertical motion for the heavy riming cases does not overlap with the range for the lightly rimed cases.

For the mature cyclones, the surface cyclone is ~10 hPa deeper than the light and moderate riming periods, with the stronger easterly winds over Long

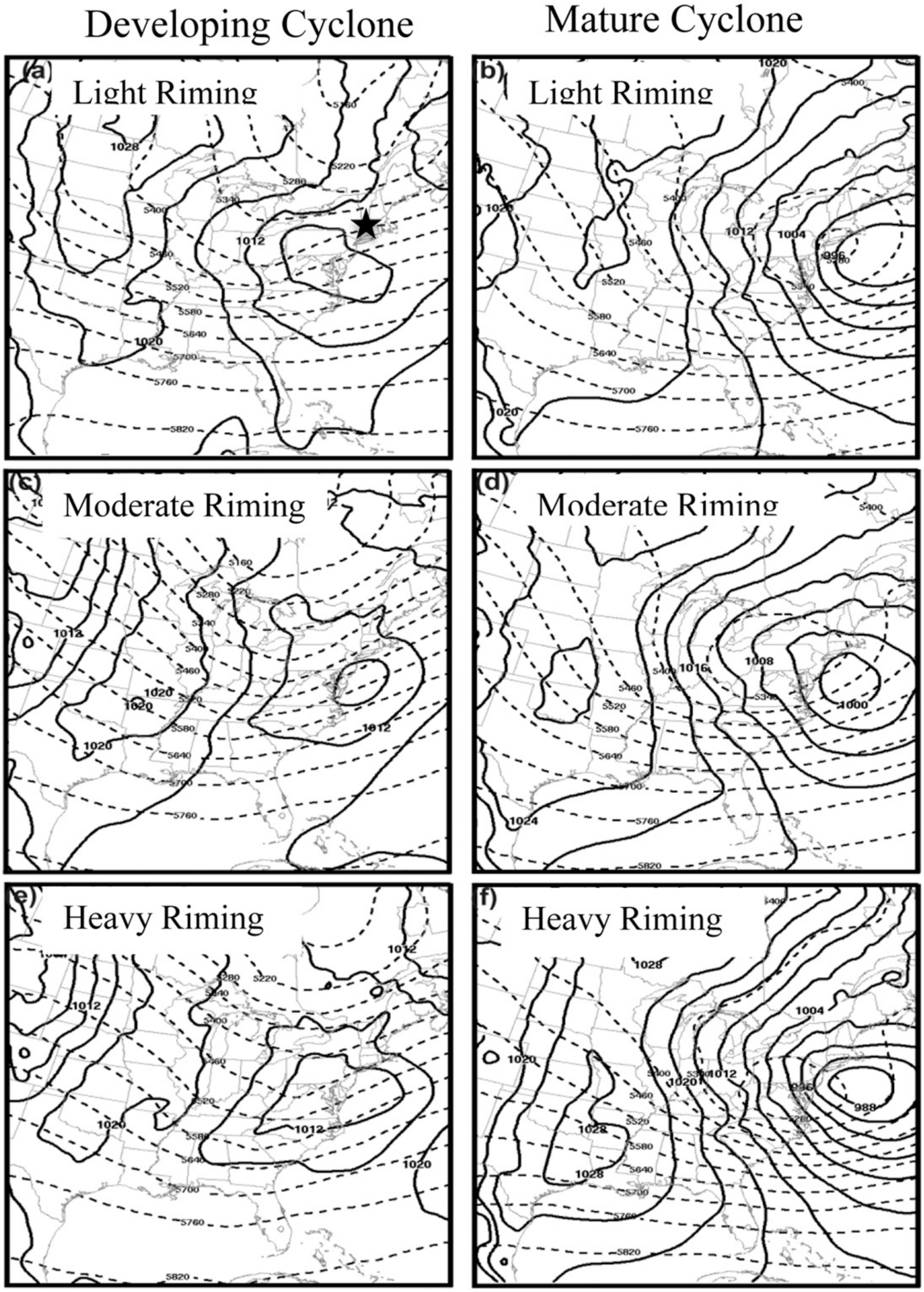

FIG. 7. 500-hPa height (contoured every 60 m) and sea level pressure (contoured ever 4 hPa) composites from hourly 13-km RUC for (a),(b) light riming periods; (c),(d) moderate riming periods; and (e),(f) heavy riming periods. (a),(c),(e) Developing cyclones and (b),(d),(f) mature cyclones. The star in (a) is the location of SBNY.

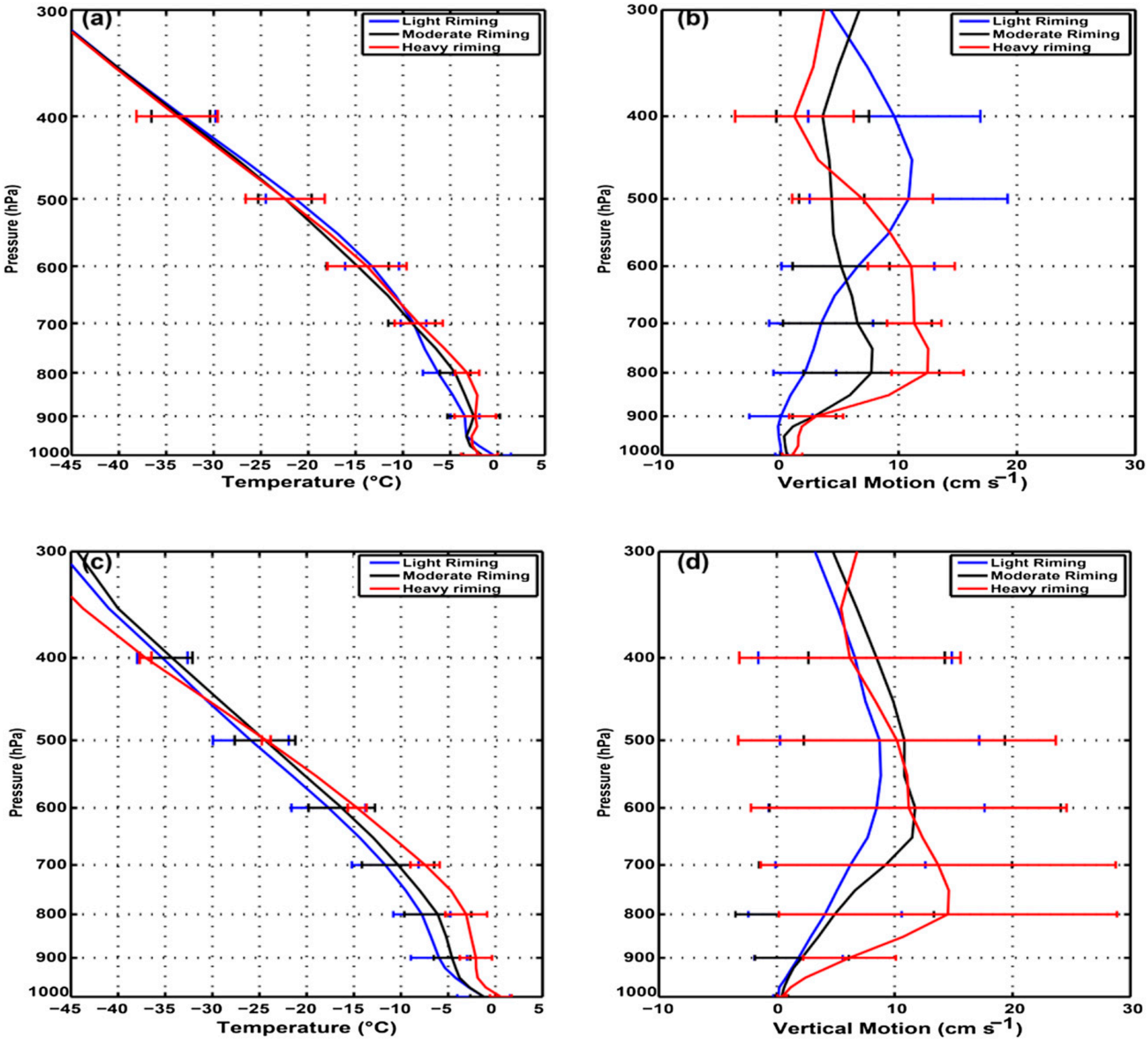

FIG. 8. 13-km RUC composite profiles of (a),(c) temperature (°C) and (c),(d) vertical motion (cm s^{-1}) for the light, moderate, and heavy riming time periods. (a),(b) Developing cyclone events and (c),(d) mature cyclone events. Horizontal bars represent the maximum and minimum values above and below the mean profile.

Island helping to advect low-level warmer air from the Atlantic and to enhance the low-level upward motion. In the mature cyclones, the temperature profile is ~2.5°C warmer than the developing storms (Fig. 8c) within a vertical motion maximum of ~14 cm s^{-1} (Fig. 8d) between 600 and 900 hPa. There is a relatively large range of vertical motions for mature cyclones, so this was not the main distinguishing factor for riming intensity. Rather, temperature explains the riming differences, since heavy riming in mature cyclones was ~1.5°C warmer in a layer from 900 to 400 hPa relative to the lightly rimed cases, with no overlap in temperature between the light and heavy riming events at 900–800 hPa.

d. Joint frequency analysis of MRR radar variables by degree of riming

Figure 9 shows the joint frequency with altitude distributions for reflectivity, Doppler velocity, and velocity spectral widths based on MRR data at SBNY during light, moderate, and heavy riming periods. Distributions are combined for developing and mature cyclones. Periods with light riming often had snow echo extending to higher altitudes than periods with heavier riming (Fig. 9, top row). The reflectivity distributions all show increases in hydrometeor reflectivities with decreasing height, indicative of growth in terms of changes in the

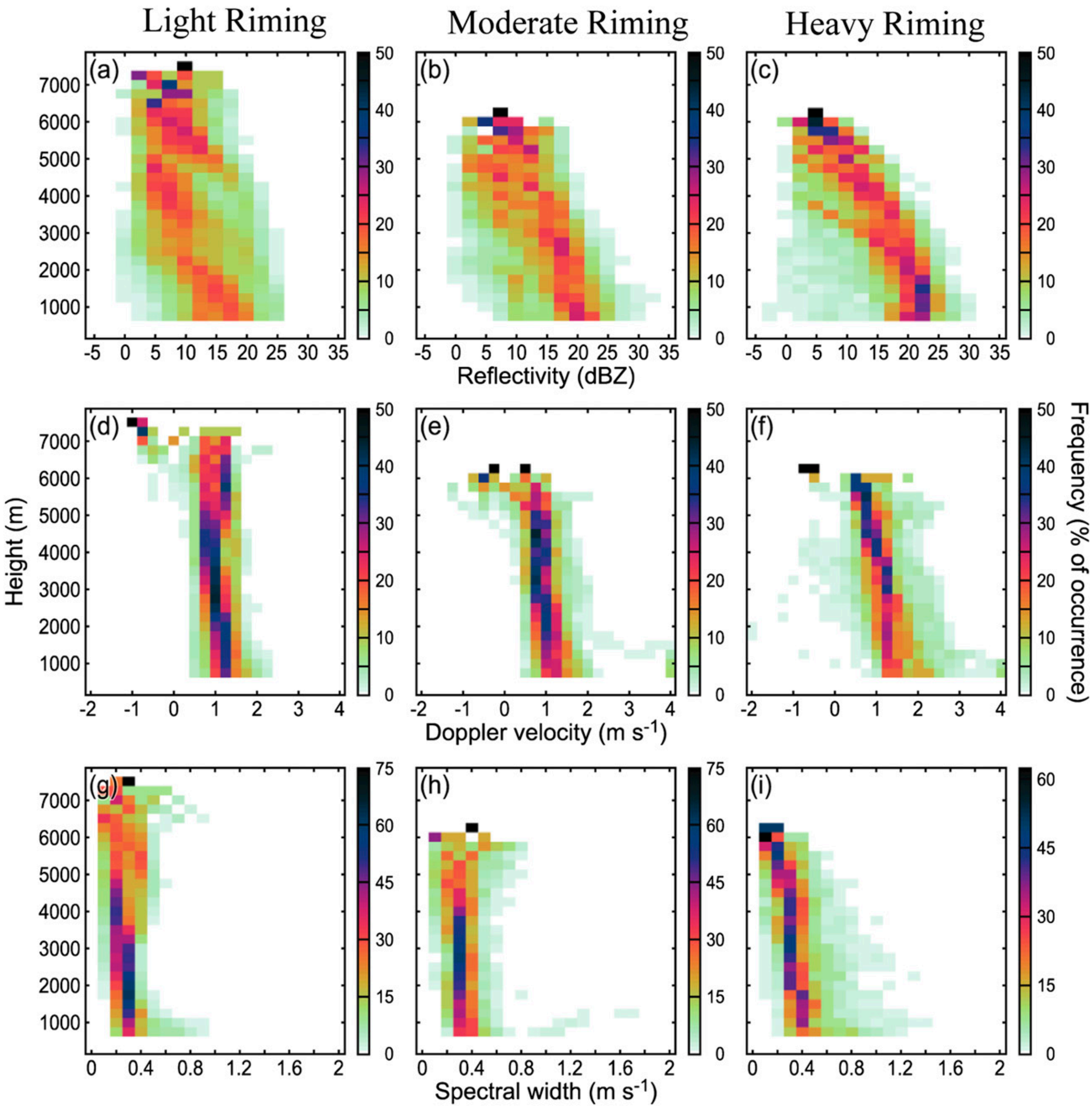

FIG. 9. Joint frequency distributions of MRR radar variables with height at SBNY for periods with light, moderate, and heavy riming. Reflectivity for the (a) light, (b) moderate, and (c) heavy riming events; Doppler velocities for the (d) light, (e) moderate, and (f) heavy riming events; and spectral width for the (g) light, (h) moderate, and (i) heavy riming events. Periods for developing and mature cyclones are combined. Downward Doppler velocity is positive.

number concentration, size, and density of snow. The low riming reflectivity distribution (Fig. 9a) shows modal reflectivity values between 5 and 10 dBZ at 4-km altitude increasing to 15–20 dBZ near the surface. In contrast, the heavy riming reflectivity distribution shows higher values aloft, with the mode centered at about 13 dBZ at 4-km altitude, and the modal reflectivity increases to over 20 dBZ near the surface. The moderate riming reflectivity distribution has intermediate values.

The combination of Doppler velocity with spectral width (a proxy for turbulence) aids in the interpretation of the velocity environment since the fall speeds of snow are variable (Locatelli and Hobbs 1974), and the Doppler velocity represents the sum of fall speed and vertical air motion. Light riming periods were characterized by Doppler velocities increasing slightly from just under to just over $1\,\mathrm{m\,s^{-1}}$ with decreasing height below 4-km altitude (Fig. 9d). The distribution of spectral widths is very narrow from 4- to 1-km altitude and the magnitude of the mode is small, $\sim 0.3\,\mathrm{m\,s^{-1}}$ consistent with weak turbulence. These are characteristics of a velocity environment without strong up- or downdrafts where the hydrometeors grow as they fall. Larger spectral width values close to the surface in Fig. 9g may be in part related to boundary layer turbulence since they have limited vertical extent. In contrast, the distributions of Doppler velocity and spectral width for heavy riming (Figs. 9f,i) have wider distributions of both Doppler velocity and spectral width below 4-km altitude indicative of the presence of stronger updrafts and downdrafts as outliers in the distributions (Yuter and Houze 1995). The modal Doppler velocities are slightly higher for heavy riming (Fig. 9f) as compared to light riming (Fig. 9d) consistent with the larger modal reflectivity values in Fig. 9c. Additionally, for heavy riming there is a tail of Doppler velocity values $>2\,\mathrm{m\,s^{-1}}$ below 1.5-km altitude indicative of higher fall speeds for the subset of heavier particles (Fig. 9f). The distributions of Doppler velocity and spectral width for moderate riming again show intermediate values and illustrate that there is a continuum of states between light and heavy riming.

Above 4-km altitude, the spectral width for the light and moderate riming periods is wider than it is at lower levels (Figs. 9g,h). This signature suggests that there may be some turbulent convective motions at these upper levels. The spectral width distribution for heavy riming periods has a broader distribution of spectral widths from 0.3 to $0.6\,\mathrm{m\,s^{-1}}$ below 5 km, which suggests turbulent motions extending to lower levels of the cloud, which can increase cloud water production and efficiency of accretional growth and riming of snow.

To illustrate the variations of reflectivity, fall speed, and spectral width for a particular case, Fig. 10 shows a time–height variation of these quantities for a snow event between 0700 and 1700 UTC 21 January 2012. After 1700 UTC 21 January, the boundary layer warmed and rain was observed at the surface. From 0900 to 1000 UTC during a period of light riming, the reflectivity increases from about 5 dBZ near detected snow echo top to 20 dBZ near the surface (Fig. 10a). The lower values of Doppler velocity near zero (upward air motion + fall speed) suggest upward motions and potentially generating cells near the echo top (Fig. 10c). The 1200 UTC 21 January 2012 sounding from KOKX had a shallow layer of potential instability between 600 and 500 hPa (not shown). As riming increased to moderate between 1130 and 1230 UTC 21 January, 15-dBZ echoes extend higher (Fig. 10a) and some short periods of higher spectral width are present (Fig. 10b). Spectral width at 3-km altitude and below noticeably increases starting about 1300 UTC and into the highlighted period with heavy riming from 1500 to 1600 UTC (Fig. 10b). Higher turbulence descended from 2700 m to the surface between 1500 and 1600 UTC 21 January, and the Doppler velocities increased to $2–3\,\mathrm{m\,s^{-1}}$ between 4 km and the surface within the heavily rimed snow (Figs. 10b,c). This suggests that the midlevel turbulence within updrafts may have enhanced the accretional growth and riming.

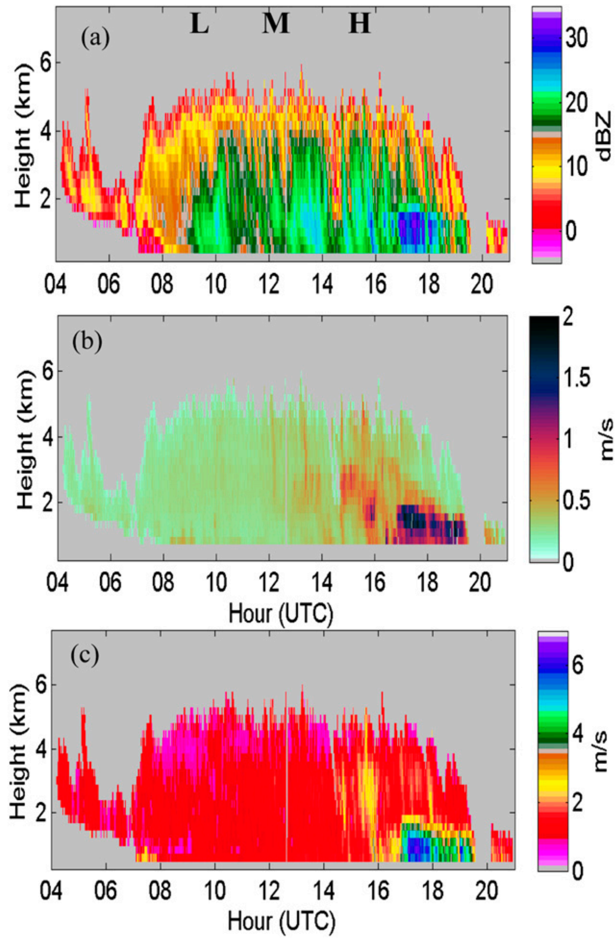

FIG. 10. Time–height plot for the MRR at SBNY from 0000 UTC 21 Jan to 0000 UTC 22 Jan 2012 showing (a) reflectivity (shaded, dBZ), (b) spectral width ($\mathrm{m\,s^{-1}}$), and (c) velocities (downward is positive, $\mathrm{m\,s^{-1}}$). Highlighted time periods when light, moderate, and heavy riming are discussed in text are shown using black boxes labeled as L, M, and H, respectively.

5. Snow-to-liquid ratio variations

Time periods with snow-to-liquid ratio less than or equal to 7:1 were categorized as having a low ratio.

TABLE 3. Time periods for the snow-to-liquid ratio subset for the developing and mature cyclones.

Case	Time period (UTC)
Developing cyclones	
Low ratio	
10 Feb 2010	0600–0800
16 Feb 2010	0700–0900
21 Jan 2012	1600–1900
11 Feb 2012	1200–1300
Medium ratio	
16 Feb 2010	0200–0600
21 Jan 2011	0700–1200
21 Feb 2011	1100–1500
21 Jan 2012	1100–1500
11 Feb 2012	1400–1700
High ratio	
21 Feb 2010	0800–1200
21 Jan 2012	0900–1000
Mature cyclones	
Low ratio	
19 Dec 2009	1700–2300
10 Feb 2010	0900–1000
10–11 Feb 2010	1500–0000
3 Mar 2010	0900–1300
5 Mar 2010	1200–1500
12 Jan 2011	0800–1000
Medium ratio	
20 Dec 2009	0000–1400
3–4 Jan 2010	2100–0300
10 Feb 2010	1100–1400
11 Feb 2010	0100–0300
26 Feb 2010	0900–1000, 1100–1300
26 Feb 2010	1800–2000
12 Jan 2011	0200–0700
12 Jan 2011	1100–1400
High ratio	
3 Jan 2010	1800–2000
26 Feb 2010	1000–1100, 1400–1700, 2100–2300

A medium ratio was defined as snow-to-liquid ratios from 8:1 to 12:1, and a high ratio was from 13:1 to 17:1. Table 3 presents the periods that are associated with the three ratio categories. Snow-to-liquid ratios reflect the relative proportions of the volume occupied by the hydrometeor that is ice or air (Roebber et al. 2003) and are in part determined by degree of riming (Power et al. 1964). Low ratios can occur in either one or both of two distinct crystal types: 1) heavily rimed hydrometeors (including graupel) or 2) simple compact crystal shapes such as needles, side planes, and bullets that are lightly rimed or not rimed. Sleet and frozen water droplets also have a low ratio. High ratios typically occur for more complex crystal shapes with air spaces within the crystal such as dendrites and plates that are either lightly or not rimed.

Observed low ratio periods exhibited both heavily rimed particles and less rimed compact habits. The low ratio periods (8 h) sampled in developing cyclones (Fig. 11a) had environments with graupel and sleet (~44%) and some side planes and bullets (28%). The low ratio periods (25 h) sampled in mature cyclones (Fig. 11b) were dominated by simple compact shapes, side planes, and bullets (~40%), as well as needles (~32%). Less than 10% of the observed snow habit in low ratio periods consists of dendrites and plates in both cyclone types.

Dendrites and plates more frequently occurred in medium and high ratio periods than low ratio periods. For medium ratio periods (20 h for developing, 38 h for mature), the frequency of dendrites and plates increases to about 50% and the frequency of side planes and bullets decreases compared to low ratio snow (Figs. 11c,d). Needles are also present at about ~20% in both the developing and mature cyclone samples (Figs. 11c,d). The sample sizes for the high ratio snow are small (5 h for developing, 8 h for mature) so these results are likely less representative than those for low and medium ratios. As expected, dendrites and plates dominate for high snow-to-liquid ratio periods at SBNY (Figs. 11e,f). The occurrence of side planes decreases from low to high ratio snow in mature cyclones. In our sample, side planes have similar frequency in both low and high ratio snow in developing cyclones.

The altitudes and strengths of upward motions in the vertical profile and the associated temperatures are both relevant for determining snow-to-liquid ratio (Roebber et al. 2003). The composites of 500-hPa height and sea level pressure, as well as the vertical profiles of temperature and vertical motion are generally consistent with the habits and riming expected during low to high ratios periods. For the developing cyclones with high ratios, SBNY is in the eastern outer region of the comma head (Fig. 3) relative to the cyclone center over the Ohio Valley (Fig. 12e), and there is a weak 500-hPa trough over the Northeast United States. Profiles at SBNY show a maximum in upward motion at midlevels (600–400 hPa) (Fig. 13b) and temperatures between $-12°$ and $-30°C$ (Fig. 13a), which favor growth of primarily side planes (~30%) and dendrites (~25%). Below 700 hPa, the combination of relatively weak upward motion and colder temperatures in high ratio periods is less favorable to riming compared to profiles for medium and low snow ratios. The mature cyclones sampled included only two events with high ratios (Table 3). These periods occurred when there was a deep closed 500-hPa low centered over SBNY (Fig. 12f), with a relatively deep (~990 hPa) surface low pressure also located over SBNY (Fig. 12f). This vertically stacked cold core low results in weak upward motion in the critical dendritic growth temperatures, while the cold temperatures favor less supercooled water and higher ratios.

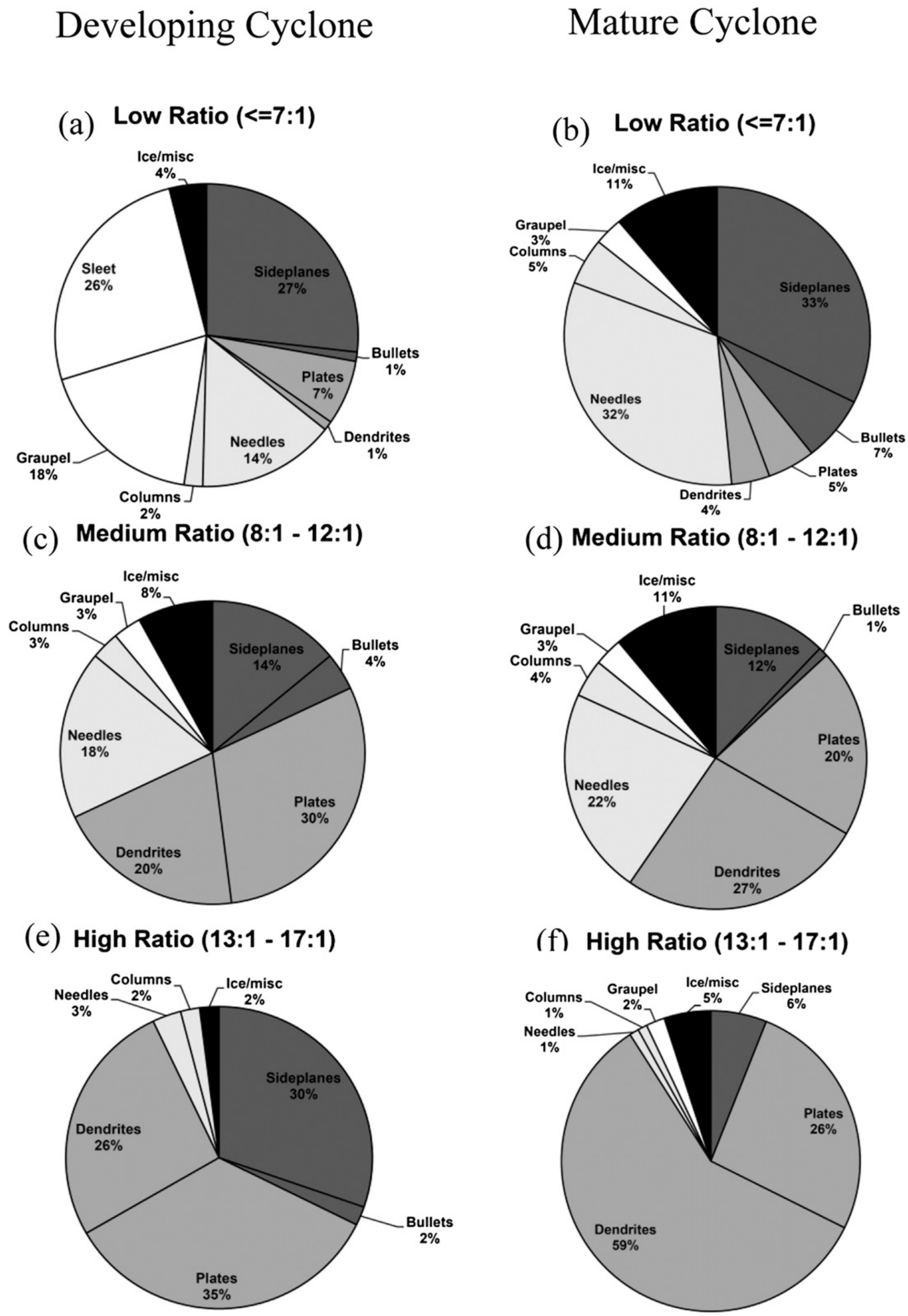

FIG. 11. (a),(b) Observed ice habit percentages in the low ratio (≤7:1) time periods; (c),(d) medium ratio (>8:1–12:1) time periods; and (e),(f) high ratio (>13:1–17:1) time periods. (a),(c),(e) Developing cyclone and (b),(d),(f) mature cyclone.

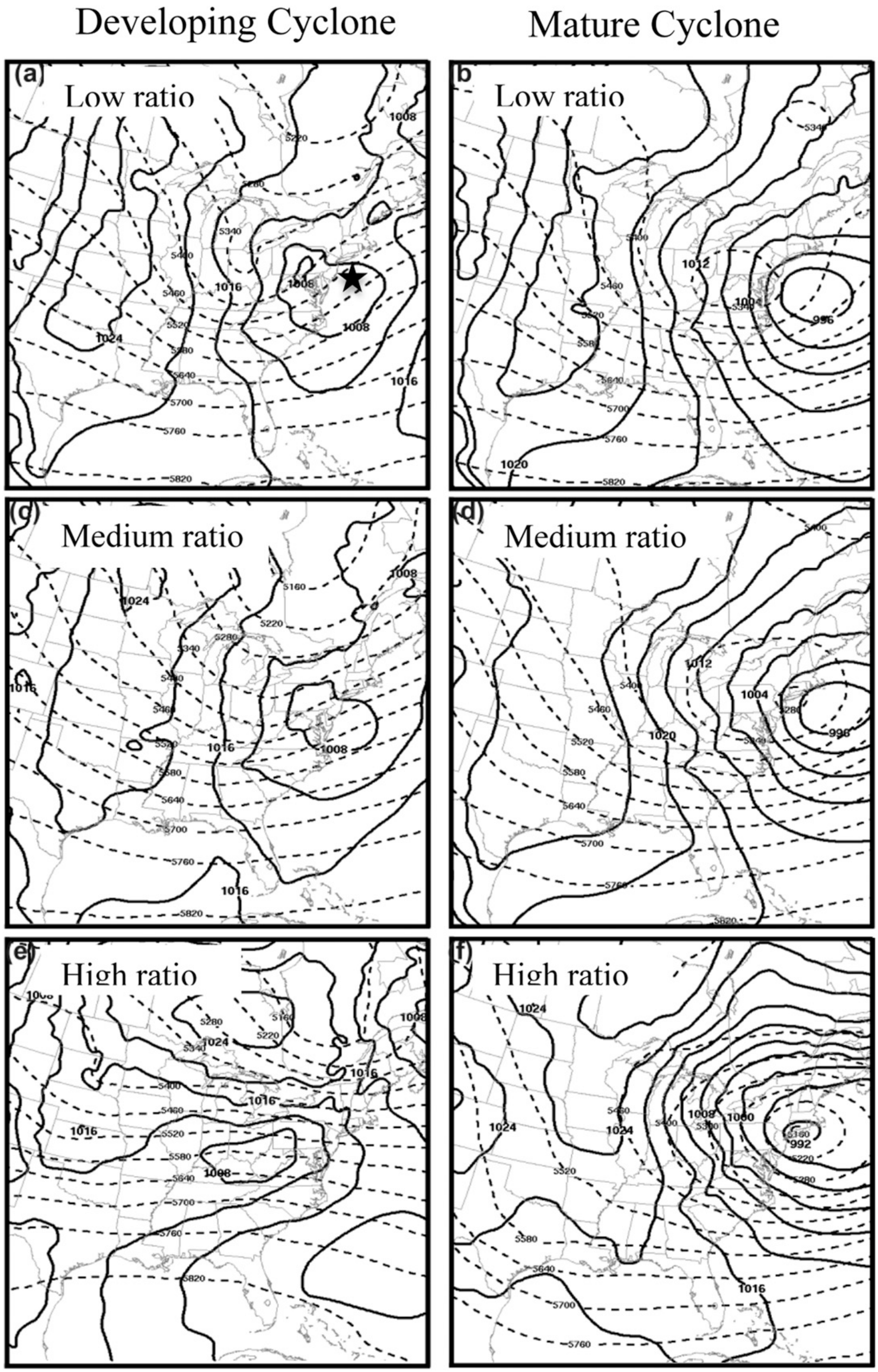

FIG. 12. As in Fig. 7, but (a),(b) low ratio periods; (c),(d) medium ratio periods; and (e),(f) high ratio periods. A low, medium, and high ratio is defined as a snow-to-liquid ratio of <7:1, 8:1–12:1, and 13:1–17:1, respectively. The star in (a) is the location of SBNY.

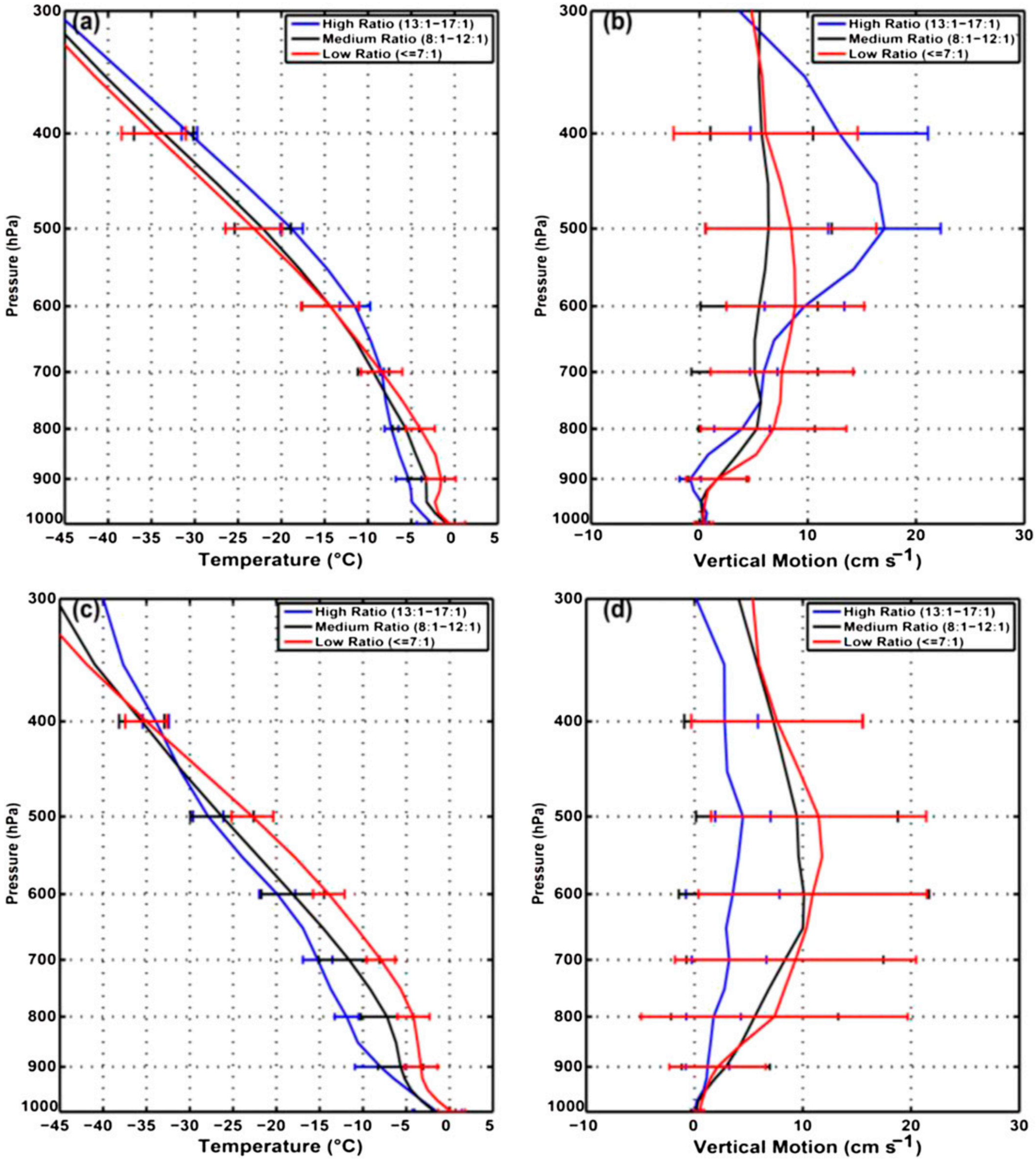

FIG. 13. As in Fig. 8, but for the low, medium, and high ratio subsets. A low, medium, and high ratio is defined as a snow-to-liquid ratio of <7:1, 8:1–12:1, and 13:1–17:1, respectively.

The composite flow patterns for the low and medium ratio periods (Figs. 12a–d) are similar to the moderate and heavily rimed composites (Figs. 7c–f). The developing surface low is located near the mid-Atlantic coast (Figs. 12a,c), closer to SBNY than during the developing cyclone high ratio periods (Fig. 12e), and there is an upper-level trough several hundred kilometers to the west of SBNY. During the mature cyclone low and medium ratio periods the surface cyclone is to the southeast of SBNY. The close proximity of the surface cyclone to SBNY results in a deep upward motion maximum (850–500 hPa) for both the developing and mature cyclones (Figs. 13b,d). In contrast to the upward motions associated with the mature high ratio periods, the average temperatures for the low ratio periods from 950 to 750 hPa were 3°–10°C higher. The higher temperatures in the low ratio events coupled with the upward motion at lower levels favors more needle growth and riming.

6. Conclusions

In situ surface observations of coexisting habits and degree of riming at SBNY had some consistent patterns among 12 snow events. This analysis represents an initial step beyond case studies (e.g., Stark et al. 2013) toward the goal of generalizing the microphysical evolution of the ice crystal habits and degree of riming within winter storms over the northeast U.S. coast. The spatial positions of the observations at SBNY were composited relative to the horizontal structure of the developing and mature cyclones. A total of 219.2 cm of snow was measured with an average degree of riming of 1.25 and snow-to-liquid ratio ranging from as low as 3:1 to as high as 17:1. Cold-type habits (side planes and bullets) commonly occurred within the outer comma head to the north and northeast of the cyclone center. In the middle of the comma head, moderately rimed dendrites, plates, and needles were observed. Close to the cyclone center, heavy riming was observed with needles and graupel. The western quadrant of the comma head had primarily plates and dendrites with little to no riming. Reinking's (1975) graupel and snow crystal observations in the Sierra Nevada did not reveal preferential locations for graupel occurrence relative to cyclone structure. Orographic processes present in the Sierra Nevada, but not at the relatively flat topography of Stony Brook, New York, may have contributed to making graupel more widespread in that previous study.

The habit types are summarized for different periods of riming intensity and ambient conditions. Periods of light riming are dominated by cold-type habits, dendrites, and plates when a weak surface low (~1008 hPa) is situated across the mid-Atlantic in the developing stage and a deeper low (~996 hPa) is located ~400 km southeast of SBNY in mature stage. The vertical motion maximum (8–10 cm s^{-1}) is between 650 and 400 hPa in temperatures from −15° to −25°C. During moderate riming periods, the vertical motion maximum (8 cm s^{-1} in developing cyclones; 11 cm s^{-1} in mature cyclones) is lower in the atmosphere (900–700 hPa in developing cyclones; 700–500 hPa in mature cyclones) and in higher temperatures (difference of 1.5°–2°C from light riming periods) and the surface cyclones are closer to SBNY (~200 km south). In a limited sample of heavy riming periods, needles and graupel are dominant with a strong vertical motion maximum (~13 cm s^{-1}) at around 800 hPa. The temperatures corresponding to the strongest vertical motions are 1.5°–2.5°C higher in heavy riming as compared to moderate riming. During heavy riming periods, there were no cold-type crystals observed and <20% of the observed habits are dendrites and plates.

The joint frequency distributions of reflectivity, spectral width, and Doppler velocity with height from a vertically pointing Ka-band radar provide further information about the environments associated with different degrees of riming observed at the surface. The reflectivity distributions all show increasing radar reflectivity with decreasing height indicative of growth in terms of changes in the number concentration, size, and density of snow. Modal reflectivity values are higher for periods of heavier riming than for light riming. The velocity environment inferred from the combination of Doppler velocity and spectral width indicates weaker vertical motions and weaker turbulence for light riming as opposed to heavy rimming periods. In heavy riming periods, the wide range of observed values of Doppler velocity and spectral width below 4 km are consistent with the presence of strong updrafts and downdrafts. The joint frequency distributions with height of the three radar-observed variables show intermediate values for moderate riming.

The habit types are also summarized for various snow-to-liquid ratio periods and ambient conditions. While high ratio periods (≥13:1 snow-to-liquid ratio) roughly correspond to those with light riming, low ratio periods (≤7:1 snow-to-liquid ratio) can occur either as heavy rimed particles or light riming of compact habits such as side planes, bullets, and needles. The low ratio/heavy riming combination occurred when the low center of developing cyclone was to the southwest of SBNY and the low ratio/compact habits combination occurred when the low center of mature cyclone was to the southeast of SBNY. Vertical motion profiles during low ratio periods favor growth through a deep layer. High ratio periods were dominated by lightly rimed plates and dendrites and occurred in the eastern outer region of the comma head for developing cyclones and when the low was centered over SBNY for mature cyclones.

Overall, this study illustrates the spatial variability in microphysics that can occur within a winter storm. The dominant locations for riming intensity and habits are dependent on the location within the cyclone comma head and the associated temperature and vertical motion patterns. This work helps refine the conceptual model of cyclone cloud structures and offers challenges to numerical models to predict these microphysical variations.

Acknowledgments. We thank the three anonymous reviewers for their constructive comments and suggestions that helped to improve the paper. We also thank Dr. Andrew Molthan for his comments on an earlier version of this manuscript. Special thanks to Dr. Gordon Taylor for allowing us the use of his microscope and camera throughout the observational portion of this study and to Andrew Hall and Spencer Rhodes for their technical support with the MRR data. This material is also based upon work supported by the National Science Foundation under Grants AGS-0908288 and AGS-1347499 (for Colle) and Grants AGS-0908420 and AGS-1347491 (for Yuter). Any opinions, findings, and conclusions or recommendations expressed in this material are those of the author(s) and do not necessarily reflect the views of the National Science Foundation.

REFERENCES

Alcott, T. I., and W. J. Steenburgh, 2010: Snow-to-liquid ratio variability and prediction at a high-elevation site in Utah's Wasatch Mountains. *Wea. Forecasting,* **25,** 323–337, doi:10.1175/2009WAF2222311.1.

Bailey, M. P., and J. Hallett, 2009: A comprehensive habit diagram for atmospheric ice crystals: Confirmation from the laboratory, AIRS II, and other field studies. *J. Atmos. Sci.,* **66,** 2888–2899, doi:10.1175/2009JAS2883.1.

Benjamin, S. G., and Coauthors, 2004: An hourly assimilation–forecast cycle: The RUC. *Mon. Wea. Rev.,* **132,** 495–518, doi:10.1175/1520-0493(2004)132<0495:AHACTR>2.0.CO;2.

Binder, P., and C. Schar, Eds., 1996: MAP—Mesoscale Alpine Programme design proposal. MAP Programme Office, 77 pp. [Available from MAP Programme Office c/o Swiss Meteorological Institute, Krähbühlstrasse 58, CH-8044 Zürich, Switzerland.]

Bjerknes, J., and H. Solberg, 1922: Life cycle of cyclones and the polar front theory of atmospheric circulation. *Geofys. Publ.,* **3,** 3–18.

Borys, R. D., D. H. Lowenthal, S. A. Cohn, and W. O. J. Brown, 2003: Mountaintop and radar measurements of anthropogenic aerosol effects on snow growth and snowfall rate. *Geophys. Res. Lett.,* **30,** 1538, doi:10.1029/2002GL016855.

Brown, M. J., J. D. Locatelli, M. T. Stoelinga, and P. V. Hobbs, 1999: Numerical modeling of precipitation cores on cold fronts. *J. Atmos. Sci.,* **56,** 1175–1196, doi:10.1175/1520-0469(1999)056<1175:NMOPCO>2.0.CO;2.

Browning, K. A., 1974: Mesoscale structure of rain systems in the British Isles. *J. Meteor. Soc. Japan,* **50,** 314–327.

Carlson, T. N., 1980: Airflow through midlatitude cyclones and the comma cloud pattern. *Mon. Wea. Rev.,* **108,** 1498–1509, doi:10.1175/1520-0493(1980)108<1498:ATMCAT>2.0.CO;2.

Cha, J., K. Chang, S. Yum, and Y. Choi, 2009: Comparison of the bright band characteristics measured by Micro Rain Radar (MRR) at a mountain and a coastal site in South Korea. *Adv. Atmos. Sci.,* **26,** 211–221, doi:10.1007/s00376-009-0211-0.

Crosier, J., and Coauthors, 2014: Microphysical properties of cold frontal rainbands. *Quart. J. Roy. Meteor. Soc.,* **140,** 1257–1268, doi:10.1002/qj.2206.

Demoz, B. B., R. Zhang, and R. L. Pitter, 1993: An analysis of Sierra Nevada winter orographic storms: Ground-based ice-crystal observations. *J. Appl. Meteor.,* **32,** 1826–1836, doi:10.1175/1520-0450(1993)032<1826:AAOSNW>2.0.CO;2.

Garvert, M. F., B. A. Colle, and C. F. Mass, 2005: The 13–14 December 2001 IMPROVE-2 event. Part I: Synoptic and mesoscale evolution and comparison with a mesoscale model simulation. *J. Atmos. Sci.,* **62,** 3474–3492, doi:10.1175/JAS3549.1.

——, B. Smull, and C. Mass, 2007: Multiscale mountain waves influencing a major orographic precipitation event. *J. Atmos. Sci.,* **64,** 711–737, doi:10.1175/JAS3876.1.

Harrold, T. W., 1973: Mechanisms influencing the distribution of precipitation within baroclinic disturbances. *Quart. J. Roy. Meteor. Soc.,* **99,** 232–251, doi:10.1002/qj.49709942003.

Hobbs, P. V., 1975: The nature of winter clouds and precipitation in the Cascade Mountains and their modification by artificial seeding. Part I: Natural conditions. *J. Appl. Meteor.,* **14,** 783–804, doi:10.1175/1520-0450(1975)014<0783:TNOWCA>2.0.CO;2.

——, T. J. Matejka, P. H. Herzegh, J. D. Locatelli, and R. A. Houze, 1980: The mesoscale and microscale structure and organization of clouds and precipitation in midlatitude cyclones. Part I: A case study of a cold front. *J. Atmos. Sci.,* **37,** 568–596, doi:10.1175/1520-0469(1980)037<0568:TMAMSA>2.0.CO;2.

Houze, R. A., P. V. Hobbs, P. H. Herzegh, and D. B. Parsons, 1979: Size distributions of precipitation particles in frontal clouds. *J. Atmos. Sci.,* **36,** 156–162, doi:10.1175/1520-0469(1979)036<0156:SDOPPI>2.0.CO;2.

Judson, A., and N. Doesken, 2000: Density of freshly fallen snow in the central Rocky Mountains. *Bull. Amer. Meteor. Soc.,* **81,** 1577–1587, doi:10.1175/1520-0477(2000)081<1577:DOFFSI>2.3.CO;2.

Keighton, S., and Coauthors, 2009: A collaborative approach to study northwest flow snow in the Southern Appalachians. *Bull. Amer. Meteor. Soc.,* **90,** 979–991, doi:10.1175/2009BAMS2591.1.

Kneifel, S., M. S. Kulie, and R. Bennartz, 2011a: A triple-frequency approach to retrieve microphysical snowfall parameters. *J. Geophys. Res.,* **116,** D11203, doi:10.1029/2010JD015430.

——, M. Maahn, G. Peters, and C. Simmer, 2011b: Observation of snowfall with a low-power FM-CW K-band radar (Micro Rain Radar). *Meteor. Atmos. Phys.,* **113,** 75–87, doi:10.1007/s00703-011-0142-z.

Lin, Y., and B. A. Colle, 2011: A new bulk microphysical scheme that includes varying degree of riming and particle habits. *Mon. Wea. Rev.,* **139,** 1036–1047, doi:10.1175/2010MWR3299.1.

Locatelli, J. D., and P. V. Hobbs, 1974: Fall speeds and masses of solid precipitation particles. *J. Geophys. Res.,* **79,** 2185–2197, doi:10.1029/JC079i015p02185.

Maahn, M., and P. Kollias, 2012: Improved micro rain radar snow measurements using Doppler spectra post processing. *Atmos. Meas. Tech.,* **5,** 2661–2673, doi:10.5194/amt-5-2661-2012.

Magono, C., and C. Lee, 1966: Meteorological classification of natural snow crystals. *J. Fac. Sci. Hokkaido Univ. Ser. 7,* **2,** 321–335.

Matejka, T. J., R. A. Houze Jr., and P. V. Hobbs, 1980: Microphysics and dynamics of clouds associated with extratropical cyclones. *Quart. J. Roy. Meteor. Soc.,* **106,** 29–56, doi:10.1002/qj.49710644704.

Matrosov, S. Y., 2007: Modeling backscatter properties of snowfall at millimeter wavelengths. *J. Atmos. Sci.,* **64,** 1727–1736, doi:10.1175/JAS3904.1.

Molthan, A., and B. A. Colle, 2012: Comparison of single and double moment microphysics schemes in the simulation of a synoptic-scale snowfall event. *Mon. Wea. Rev.,* **140,** 2982–3002, doi:10.1175/MWR-D-11-00292.1.

——, ——, W. A. Petersen, S. W. Nesbitt, and D. Hudak, 2010: Evaluating the snow crystal size distribution and density assumptions within a single-moment microphysics scheme. *Mon. Wea. Rev.,* **138,** 4254–4267, doi:10.1175/2010MWR3485.1.

Mosimann, L., E. Weingartner, and A. Waldvogel, 1994: An analysis of accreted drop sizes and mass on rimed snow crystals. *J. Atmos. Sci.,* **51,** 1548–1558, doi:10.1175/1520-0469(1994)051<1548:AAOADS>2.0.CO;2.

Novak, D., and B. A. Colle, 2012: Diagnosing snowband predictability using a multimodel ensemble system. *Wea. Forecasting,* **27,** 565–585, doi:10.1175/WAF-D-11-00047.1.

——, ——, and S. E. Yuter, 2008: High-resolution observations and model simulations of the life cycle of an intense mesoscale snowband over the Northeastern United States. *Mon. Wea. Rev.,* **136,** 1433–1456, doi:10.1175/2007MWR2233.1.

Peters, G., B. Fischer, and T. Andersson, 2002: Rain observations with a vertically looking Micro Rain Radar (MRR). *Bor. Environ. Res.,* **7,** 353–362.

Petersen, W. A., and Coauthors, 2007: NASA GPM/PMM participation in the Canadian CloudSat/CALIPSO validation project C3VP: Physical process studies in snow. *33rd Conf. on Radar Meteorology,* Cairns, Australia, Amer. Meteor. Soc., P12A.8. [Available online at https://ams.confex.com/ams/33Radar/techprogram/paper_123652.htm.]

Power, B. A., P. W. Summers, and J. d'Avignon, 1964: Snow crystal forms and riming effects as related to snowfall density and general storm conditions. *J. Atmos. Sci.,* **21,** 300–305, doi:10.1175/1520-0469(1964)021<0300:SCFARE>2.0.CO;2.

Prat, O. P., and A. P. Barros, 2010: Ground observations to characterize the spatial gradients and vertical structure of orographic precipitation—Experiments in the inner region of the Great Smoky Mountains. *J. Hydrol.,* **391,** 141–156, doi:10.1016/j.jhydrol.2010.07.013.

Rauber, R. M., 1987: Characteristics of cloud ice and precipitation during wintertime storms over the mountains of northern Colorado. *J. Climate Appl. Meteor.,* **26,** 488–524, doi:10.1175/1520-0450(1987)026<0488:COCIAP>2.0.CO;2.

——, and L. O. Grant, 1986: The characteristics and distribution of cloud water over the mountains of northern Colorado during winter-time storms. Part II: Spatial distribution and microphysical characteristics. *J. Climate Appl. Meteor.,* **25,** 489–504, doi:10.1175/1520-0450(1986)025<0489:TCADOC>2.0.CO;2.

——, ——, D. X. Feng, and J. B. Snider, 1986: The characteristics and distribution of cloud water over the mountains of northern Colorado during wintertime storms. Part I: Temporal variations. *J. Climate Appl. Meteor.,* **25,** 468–488, doi:10.1175/1520-0450(1986)025<0468:TCADOC>2.0.CO;2.

Reinking, R. F., 1975: Formation of graupel. *J. Appl. Meteor.,* **14,** 745–754, doi:10.1175/1520-0450(1975)014<0745:FOG>2.0.CO;2.

——, 1979: The onset and early growth of snow crystals by accretion of droplets. *J. Atmos. Sci.,* **36,** 870–881, doi:10.1175/1520-0469(1979)036<0870:TOAEGO>2.0.CO;2.

Reynolds, D. W., and A. S. Dennis, 1986: A review of the Sierra Cooperative Pilot Project. *Bull. Amer. Meteor. Soc.,* **67,** 513–523, doi:10.1175/1520-0477(1986)067<0513:AROTSC>2.0.CO;2.

Rinehart, R. E., 2004: *Radar for Meteorologists.* 4th ed. Rinehart Publications, 482 pp.

Roebber, P. J., S. L. Bruening, D. M. Schultz, and J. V. Cortinas Jr., 2003: Improving snowfall forecasting by diagnosing snow density. *Wea. Forecasting,* **18,** 264–287, doi:10.1175/1520-0434(2003)018<0264:ISFBDS>2.0.CO;2.

Rutledge, S. A., and P. V. Hobbs, 1983: The mesoscale and microscale structure and organization of clouds and precipitation in midlatitude cyclones. VIII: A model for the ''seeder-feeder'' process in warm-frontal rainbands. *J. Atmos. Sci.,* **40,** 1185–1206, doi:10.1175/1520-0469(1983)040<1185:TMAMSA>2.0.CO;2.

Ryan, B. F. D., E. R. Wishart, and D. E. Shaw, 1976: The growth rates and densities of ice crystals between −3°C and −21°C. *J. Atmos. Sci.,* **33,** 842–850, doi:10.1175/1520-0469(1976)033<0842:TGRADO>2.0.CO;2.

Shapiro, M. A., and D. Keyser, 1990: Fronts, jet streams and the tropopause. *Extratropical Cyclones: The Erik Palmén Memorial Volume,* C. W. Newton and E. O. Holopainen, Eds., Amer. Meteor. Soc., 167–191.

Sienkiewicz, J. M., J. D. Locatelli, P. V. Hobbs, and B. Geerts, 1989: Organization and structure of clouds and precipitation on the mid-Atlantic coast of the United States. Part II: The mesoscale and microscale structures of some frontal rainbands. *J. Atmos. Sci.,* **46,** 1349–1364, doi:10.1175/1520-0469(1989)046<1349:OASOCA>2.0.CO;2.

Stark, D., B. A. Colle, and S. E. Yuter, 2013: Observed microphysical evolution for two East Coast winter storms and the associated snow bands. *Mon. Wea. Rev.,* **141,** 2037–2057, doi:10.1175/MWR-D-12-00276.1.

Stewart, R. E., G. A. Isaac, and R. W. Crawford, 1995: Some characteristics of the precipitation formed within winter storms over eastern Newfoundland. *Atmos. Res.,* **36,** 17–37, doi:10.1016/0169-8095(94)00004-W.

Stoelinga, M. T., and Coauthors, 2003: Improvement of microphysical parameterization through observational verification experiment. *Bull. Amer. Meteor. Soc.,* **84,** 1807–1826, doi:10.1175/BAMS-84-12-1807.

——, P. V. Hobbs, J. D. Locatelli, and C. P. Woods, 2007: The occurrence of ''irregular'' ice particles in stratiform clouds. *J. Atmos. Sci.,* **64,** 2740–2750, doi:10.1175/JAS3962.1.

Super, A. B., and E. W. Holroyd III, 1997: Snow accumulation algorithm for the WSR-88D radar: Second annual report. Bureau Reclamation Tech. Rep. R-97-05, U.S. Dept. of Interior, Denver, CO, 77 pp. [Available from National Technical Information Service, 5285 Port Royal Rd., Springfield, VA 22161.]

Takahashi, T., T. Endoh, and G. Wakahoma, 1991: Vapor diffusional growth of free-falling snow crystals. *J. Meteor. Soc. Japan,* **69,** 15–30.

Xie, X., U. Löhnert, S. Kneifel, and S. Crewell, 2012: Snow particle orientation observed by ground-based microwave radiometry. *J. Geophys. Res.,* **117,** D02206, doi:10.1029/2011JD016369.

Yuter, S. E., and R. A. Houze Jr., 1995: Three-dimensional kinematic and microphysical evolution of Florida cumulonimbus. Part II: Frequency distributions of vertical velocity, reflectivity, and differential reflectivity. *Mon. Wea. Rev.,* **123,** 1941–1963, doi:10.1175/1520-0493(1995)123<1941:TDKAME>2.0.CO;2.